Unclassified

SECURITY CLASSIFICATION OF THIS PAGE

REPORT DOCUMENTATION PAGE

1a. REPORT SECURITY CLASSIFICATION **AD-A227 546**	1b. RESTRICTIVE MARKINGS
	3 DISTRIBUTION / AVAILABILITY OF REPORT Approved for public release; Distribution unlimited
	5. MONITORING ORGANIZATION REPORT NUMBER(S) GL-TR-90-0249
6a. NAME OF PERFORMING ORGANIZATION Geophysics Laboratory	6b. OFFICE SYMBOL (*If applicable*) OPC
6c. ADDRESS (*City, State, and ZIP Code*) Hanscom AFB Massachusetts 01731-5000	7a. NAME OF MONITORING ORGANIZATION 7b. ADDRESS (*City, State, and ZIP Co*)
8a. NAME OF FUNDING / SPONSORING ORGANIZATION	8b. OFFICE SYMBOL (*If applicable*)
8c. ADDRESS (*City, State, and ZIP Code*)	9 PROCUREMENT INSTRUMENT IDENTIFICATION NUMBER

DTIC ELECTE OCT 10 1990 S D

10 SOURCE OF FUNDING NUMBERS			
PROGRAM ELEMENT NO.	PROJECT NO.	TASK NO.	WORK UNIT ACCESSION NO.
61102F	2311	G7	01

11 TITLE (*Include Security Classification*)
Capabilities of the AFGL Mosaic Array Spectrometer-Ten-Micron Spectra of Bright Infrared Stars

12 PERSONAL AUTHOR(S)
Paul D. LeVan

13a. TYPE OF REPORT	13b. TIME COVERED	14. DATE OF REPORT (*Year, Month, Day*)	15 PAGE COUNT
Reprint	FROM _____ TO _____	1990 September 28	11

16 SUPPLEMENTARY NOTATION
Reprinted from the Publications of the Astronomical Society of the Pacific (Vol. 102, No. 648, February 1990)

17. COSATI CODES		
FIELD	GROUP	SUB-GROUP

18. SUBJECT TERMS (*Continue on reverse if necessary and identify by block number*)
Instrumentation-array detectors
IR Spectroscopy

19. ABSTRACT (*Continue on reverse*)

A 9- to 14-μm slit spectrometer employing a novel mosaic array of 58 × 62 detectors is described. The spectrometer has been used on the University of Wyoming 2.3-m telescope with a 0".9 per pixel (reimaged) plate scale to obtain spectra of long-period variable stars. We characterize the instrumental spectral resolution and spatial point-spread function using spectra and spatial profiles extracted from spectral images of the variable stars. ~~In order~~ to evaluate the effectiveness of ~~our~~ data-acquisition and reduction procedures, ~~our~~ spectra are compared with examples found in the Atlas of IRAS Low Resolution Spectra. The comparisons are made for single representatives of each of three diverse object classes—oxygen-rich stars with strong silicate feature emission, carbon-rich stars with silicon carbide emission, and late-type stars exhibiting photospheric continuum radiation. ~~We~~ conclude that: (1) The IRAS and array spectrometer spectra are in qualitative agreement if account is taken of the extension of the silicate feature flux to wavelengths shortward of the 9-μm cut-on wavelength of our instrument. (2) The spectral resolution of our spectrometer is as expected for the slit width employed. (3) The width of the spatial point-spread function is nearly as good as the design goal. (4) The formal uncertainties of our data points are high even when the relatively low responsivity of the mosaic array is considered and are suggestive of system noise limited performance.

20. DISTRIBUTION / AVAILABILITY	21. ABSTRACT SECURITY CLASSIFICATION
☐ UNCLASSIFIED/UNLIMITED ☒ SAME AS RPT. ☐ DTIC USERS	Unclassified

22a. NAME OF RESPONSIBLE INDIVIDUAL	22b. TELEPHONE (*Include Area Code*)	22c. OFFICE SYMBOL
Paul D. LeVan	(617) 377-4550	OPC

DD FORM 1473, 84 MAR

83 APR edition may be used until exhausted.
All other editions are obsolete.

SECURITY CLASSIFICATION OF THIS PAGE

Unclassified

DISCLAIMER NOTICE

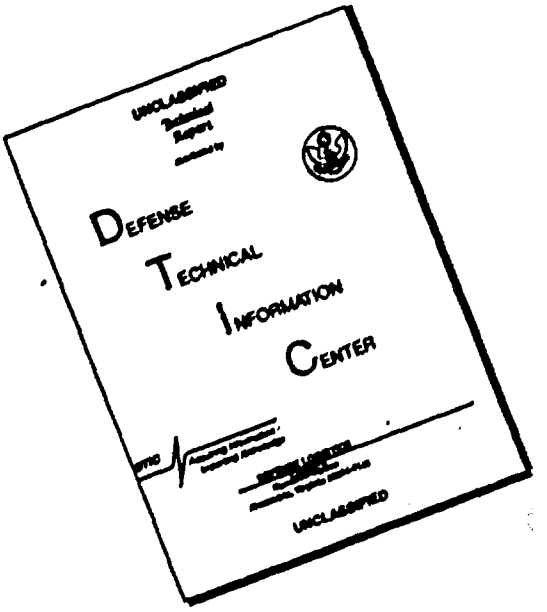

THIS DOCUMENT IS BEST QUALITY AVAILABLE. THE COPY FURNISHED TO DTIC CONTAINED A SIGNIFICANT NUMBER OF PAGES WHICH DO NOT REPRODUCE LEGIBLY.

REPRINT

CAPABILITIES OF THE AFGL MOSAIC ARRAY SPECTROMETER—TEN-MICRON SPECTRA OF BRIGHT INFRARED STARS

PAUL D. LEVAN

Reprinted from the *Publications of the Astronomical Society of the Pacific*
(Vol. 102, No. 648, February 1990)

Publications of the Astronomical Society of the Pacific
102: 190–197 February 1990

CAPABILITIES OF THE AFGL MOSAIC ARRAY SPECTROMETER—TEN-MICRON SPECTRA OF BRIGHT INFRARED STARS

PAUL D. LEVAN

Geophysics Laboratory (Air Force Systems Command), Hanscom Air Force Base, Massachusetts 01731-5000

Received 1989 July 25, revised 1989 November 13

ABSTRACT

A 9- to 14-μm slit spectrometer employing a novel mosaic array of 58 × 62 detectors is described. The spectrometer has been used on the University of Wyoming 2.3-m telescope with a 0".9 per pixel (reimaged) plate scale to obtain spectra of long-period variable stars. We characterize the instrumental spectral resolution and spatial point-spread function using spectra and spatial profiles extracted from spectral images of the variable stars. In order to evaluate the effectiveness of our data-acquisition and reduction procedures, our spectra are compared with examples found in the Atlas of IRAS Low Resolution Spectra. The comparisons are made for single representatives of each of three diverse object classes—oxygen-rich stars with strong silicate feature emission, carbon-rich stars with silicon carbide emission, and late-type stars exhibiting photospheric continuum radiation. We conclude that: (1) The IRAS and array spectrometer spectra are in qualitative agreement if account is taken of the extension of the silicate feature flux to wavelengths shortward of the 9-μm cut-on wavelength of our instrument. (2) The spectral resolution of our spectrometer is as expected for the slit width employed. (3) The width of the spatial point-spread function is nearly as good as the design goal. (4) The formal uncertainties of our data points are high even when the relatively low responsivity of the mosaic array is considered and are suggestive of system noise limited performance.

Key words: instrumentation–array detectors–IR spectroscopy

1. Introduction

Recent examples of the use of mosaic infrared arrays in ground-based astronomical cameras in the ten-micron region are readily found in the literature (Arens *et al.* 1984, Bloemof, Townes, and Vanderwyck 1984, Tresch-Fienberg *et al.* 1987, Gezari *et al.* 1988). However, such arrays also lend themselves nicely to long-slit spectroscopic applications for which radiation is dispersed along one of the array axes. Array slit spectrometers have a substantial advantage over single-detector wavelength scanning spectrometers since all wavelength elements are measured simultaneously. Hence, the shape of the spectrum is unaffected by variations in atmospheric transmission. Using a two-dimensional array in our spectrometer also permits the acquisition of long-slit spectra of extended sources.

The design of the prism spectrometer discussed here is similar in its choice of dispersing element to a discrete bolometer array spectrometer built by Gezari, Hackwell, and Smith (1976); our design is discussed in some detail in workshop proceedings (LeVan and Tandy 1987, hereafter Paper I; LeVan 1989). Here we briefly review the design, discuss upgradings to the spectrometer, and describe the results of recent observing runs. After reviewing the instrument and telescope tests, we next discuss the spectra obtained for our program stars. Next, observed noise characteristics are compared with those expected for a mosaic array operated under background-limited conditions. Finally, the spatial point-spread function is determined from monochromatic profiles of the program star exposures.

2. The Spectrometer

2.1 *Mosaic Array Clocking*

The detector array is a Santa Barbara Research Center (SBRC) 58 by 62 pixel Si:Ga photoconductor array "Indium bump bonded" to a CRC-228 Direct Read Out (DRO) multiplexer, whose properties are listed in Table 1. A circuit diagram for one of the 1798 pixel unit cells is shown in Figure 1. The DRO has two signal output lines. Each line is driven by an on-chip MOSFET source follower circuit, and a single array address code transfers the signal simultaneously from each of two adjacent pixels. Because of the spectral resolution of the spectrometer and the high background photon rates in the thermal infrared, pixels are clocked continuously at 333 kHz, giving a 3 μsec pixel "window" during which δ-Reset Sampling (DRS) may be performed. Source follower bias voltages and load resistance values were optimized to allow for

TABLE 1

Mosaic Array Attributes

Pixel format.....	58x62
Pixel spacing.....	75 μm
Photoconductor material..	Si:Ga
Multiplexer read mode[a]...	Random access; direct output
Multiplex ratio.....	1798 pixels / output channel
Well capacity.....	$3x10^6$ e-
Responsivity[b].....	< 0.4 A/W
Uniformity.....	< 5 % rms

[a]Read-out noise is below LSB of 12 bit full-well conversion

[b]Manufacturer goal of high pixel response uniformity was obtained at the expense of lowered responsivity (private communication with manufacturer, Santa Barbara Research Corporation).

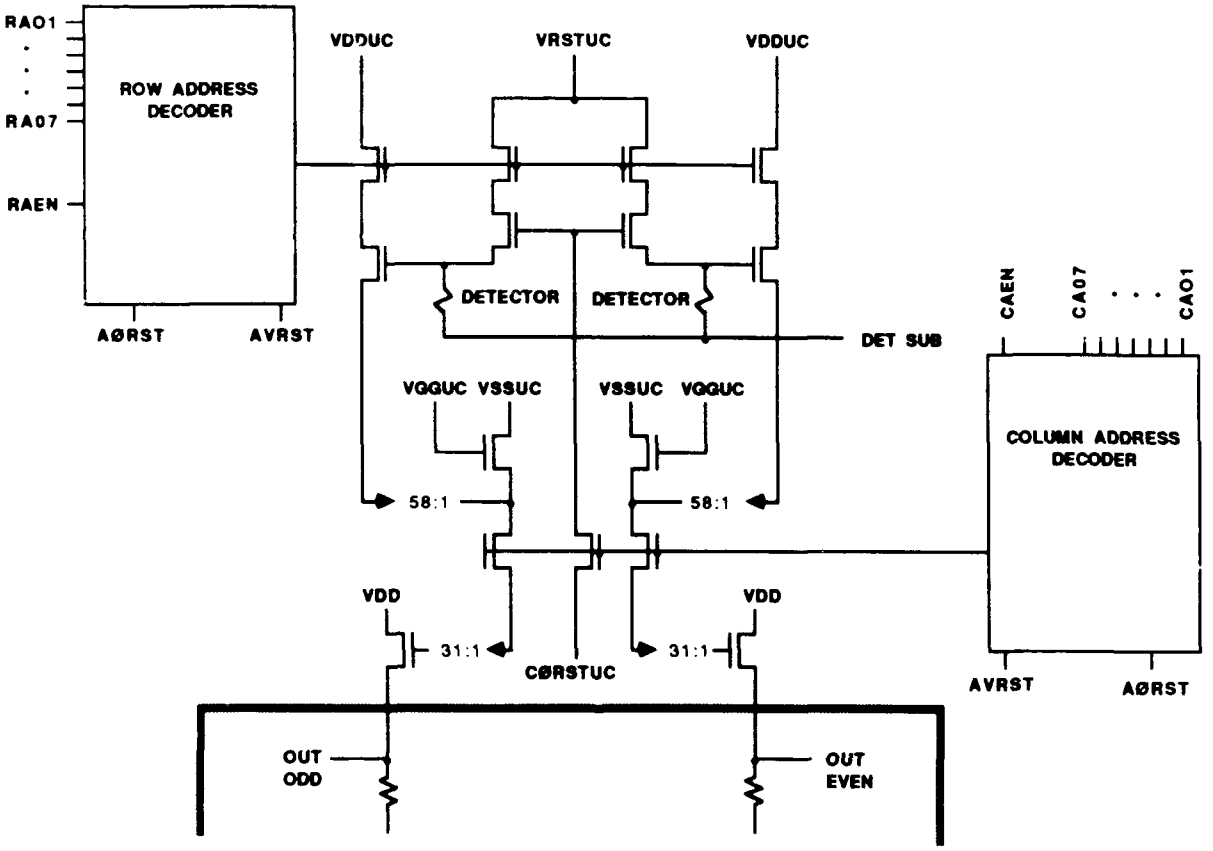

FIG. 1—Circuit drawing of one of 1798 total pixel unit cells (UC) shown with the address electronics and two source followers. Acronyms refer to bias and clock voltages supplied externally via the chip carrier: RA-n and CA-n refer to row and column address clocks. VDD, VGG, and VSS are the usual MOSFET terminology for drain, gate, and source bias voltage. AØRST denotes the address reset clock voltage that is required prior to a new address selection, and CØRST is the signal charge reset clock voltage. Load resistors for biasing the two source followers that are shown below the shaded border are supplied by the user at an off-chip location.

settling of signals during the clamp and sample of DRS. The integration time per pixel, equal to the clock period multiplied by the number of pixels per output line (1798), is 5.4 msec. Further details on the laboratory cryogenic

(10 K) testing of the array are contained in Paper I.

2.2 *The Coaddition Electronics*

Electronics for real-time coadditions of digitized array frames is based on Arithmetic Logic Units (ALUs) and was designed at the Air Force Geophysics Laboratory (AFGL). The ALU design was selected over a microprocessor-based design to allow for higher frame coaddition rates (see also Paper I). The coaddition electronics provides two separate RAM blocks of 3596 20-bit memory sites to allow for the standard IR astronomy technique of secondary mirror chopping of the source and blank sky. Coaddition suppression after each chop during the settle time of the secondary mirror prevents corruption of the summed frames. The register contents corresponding to the two telescope chop positions are differenced by the ALUs and transferred to a minicomputer for storage on hard disk before overflow of the 20-bit RAM block (fewer than 256 array frames).

2.3 *Electronics Testing*

Early laboratory testing disclosed significant clocking noise on the common analog and digital electronics grounds at the level of several bits of our 12-bit A to D converter and higher than the shot noise of a full pixel well. This resulted in our redesigning the analog electronics boards with considerable attention to isolation of the digital, bias voltage, and signal grounds. The two A to D converters were also upgraded to improved 16-bit devices with front-end sample and hold and a 2.7-μsec conversion time (Analogic Corp., Wakefield, MA). The upgraded circuitry is used in an equivalent 12-bit mode.

A problem that affected initial observing runs was electronic "spiking" of a significant percentage of the pixels before transfer of the summed frames to the computer. (Software corrections for spiking were discussed in LeVan and Sloan (1987).) Because of their predominance on only one of the two output channels, the origin of the spikes was determined to be the digital electronics. It was further determined by repeating the transfer of data differences between registers corresponding to the two telescope chop positions that the spiking occurred during data acquisition. Subsequent changes in the relative timing of the A to D converter data latching pulses sent to the two "chop" registers significantly reduced the spiking in the affected channel.

2.4 *Prism Spectrometer Optics*

The optics design summarized in Table 2 is based on a NaCl prism. A prism was selected as the dispersing element for operation over a broad wavelength range (9 to 14 μm) over which a grating efficiency would vary substantially. Our design has no cryogenically cooled moving parts. However, a simple cold blocking shutter is recommended for future designs to facilitate testing. In constructing the optics (Sensors Systems Group, Waltham, MA) care was taken to stress relieve the mirrors at the three substrate attachment points. This design was found to have good alignment stability between room temperature and 10 K. A picture of the optical assembly is shown in Figure 2. A detailed, scaled schematic of the ray trace is given in Paper I.

3. Data Acquisition

Setup at the observing site for infrared observations involves a range of procedures too numerous to mention; we concentrate below on those aspects of the setup specific to our array spectrometer.

3.1 *Observing Setup: Electronics*

The relative phases of a 333 kHz master clock and three subsidiary clocks are adjusted within the 3-μsec "pixel window", by displaying the pixel signals resulting from δ-reset sampling on an oscilloscope. The pixel signal reset clock pulse is delayed relative to the pixel address pulse to allow for settling of the signal level. The clamp pulse (which restores the signal to the zero voltage level) is delayed to just prior to pixel reset. The sample pulse initiates both sample and hold and the A to D conversion, as discussed in Section 2.3. The relative timing of the sample clock is delayed to the end of the pixel "window" (just prior to the new pixel address). The reset pixel signal settles in the form of a linear ramp to a pedestal value; the procedure outlined here allows a time interval sufficiently long to accommodate increased background or bright source signals that require proportionally longer settle times. Our electronics also generates a telescope secondary mirror chop waveform, ensuring synchronization with the array clocking. We tune the amplitude (27") and offset of the chop signal square wave using the signal from the mirror position transducer. A check is made for cancellation of the background signal in the positive and negative chop registers.

TABLE 2

Prism Spectrometer Attributes and Spectral Dispersion

Pixel	x(mm)	λ(μm)
1	0.04	8.9
15	1.10	10.7
30	2.24	12.3
45	3.38	13.7
60	4.52	14.5

Prism material.....	NaCl
$F_{collimator}$.....	270 mm
F_{camera}.....	75 mm
Lyot stop diameter..	10 mm
Slit dimensions.....	0.9x16 mm
	3.3x58 pixels

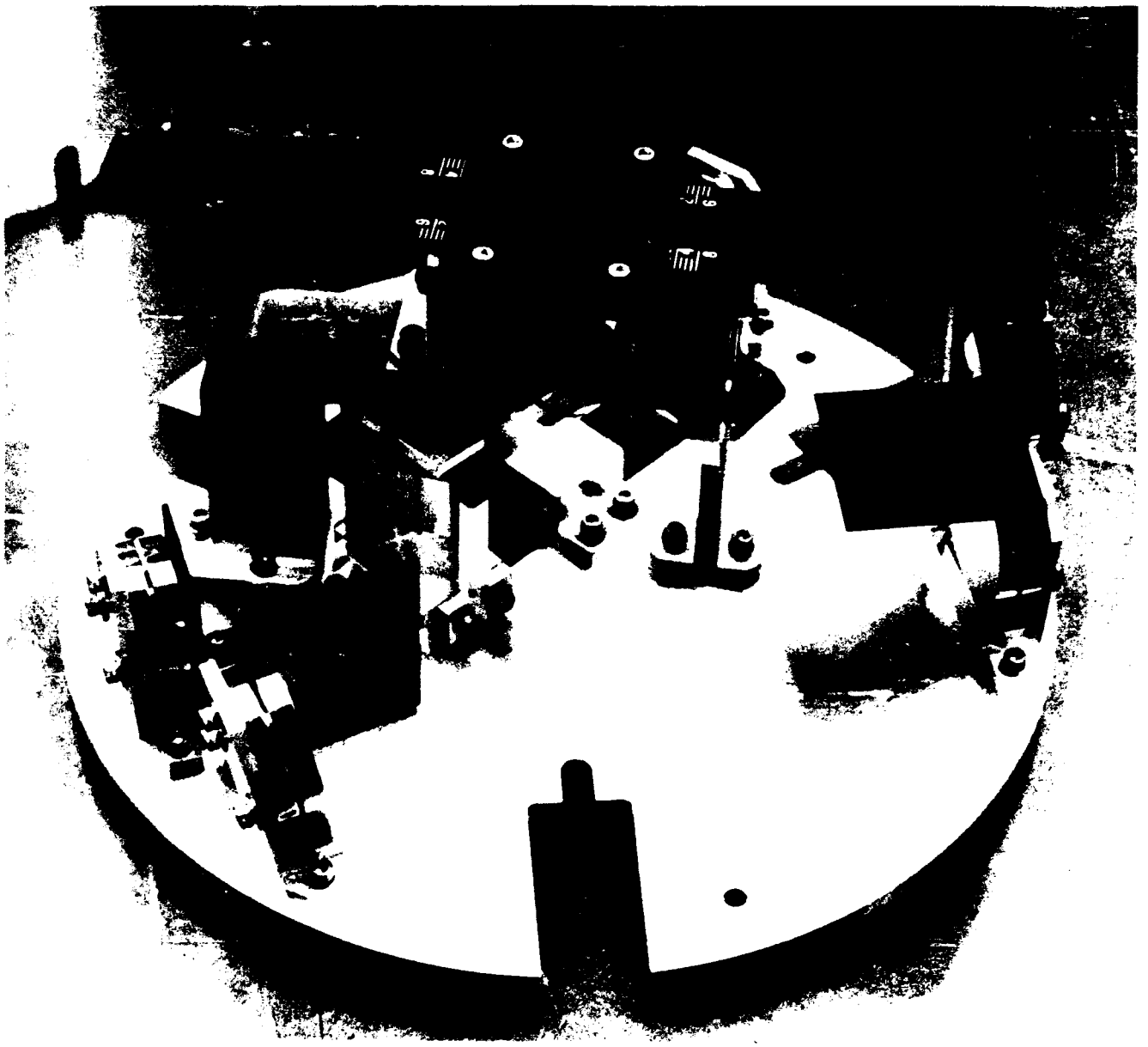

FIG. 2—The spectrometer optics, shown inverted relative to its attitude as mounted in the dewar. The material used for construction is Al; the mirror surfaces are coated with Ni. Gaps visible in the mirror assemblies provide stress relief by decoupling the mirror surfaces from the substrate mounting points. The NaCl prism is held in place with spring steel. The assembly was built to our design by Sensors System Group of Waltham, MA.

3.2 *Observing Setup: Optical Alignment*

Optical alignment consists of ensuring that the dewar field of view is centered on the telescope secondary mirror. This is accomplished using the signal of a selected pixel resulting from a warm radiation source positioned at the telescope secondary mirror. By displaying this signal on an oscilloscope it may be maximized by tilting a reflecting mirror. The widespread alternative method of adjustment of the reflecting mirror for minimum background signal *without the warm radiation source* was attempted without success. This may be due to scattering internal to the spectrometer of an appreciable component of background signal from outside of the reflecting mirror solid angle.

3.3 *Background Subtraction*

Subtraction of the sky and telescope background from the source frames is effectuated by chopping the secondary mirror of the telescope at 3 Hz. The chop direction is along the north/south axis as is the orientation of the

spectrometer slit. The chop amplitude is one-half the 54″ slit length. After seven pairs of source and blank sky chops, data collection is suspended while the differences of the frames coadded into the two chop registers are transferred to computer. This sequence is repeated 20 times for a fixed telescope position. The telescope is then nodded. Care was taken in adjusting the chop and nod amplitudes since any mismatch between them results in a spatial smearing of the source on combination of the positive and negative source frames. Nodding the telescope removes first-order spatial variation of the background. The 20 frame transfers per telescope nod position are transported off the mountain for subsequent processing.

3.4 *Optical Calibration: Positional*

The array plate scale and wavelength calibrations relate to array pixel spacing and optics magnification and dispersion listed in Table 2. The array plate scale was verified by moving a point source by fixed telescope pointing increments. The 0.″9 per pixel slope of the fit to the point-source spatial peaks and telescope pointing offsets is consistent with the telescope plate scale (3.″27 mm $^{-1}$), the pixel spacing, and the spectrometer magnification.

3.5 *Optical Calibration: Spectral*

Polystyrene film was inserted into the telescope beam at the dewar window with a background source in view. The polystyrene spectrum shown in the lower panel of Figure 3 was generated as the ratio of background source spectra with and without polystyrene in the beam; also shown is a reference spectrum synthesized from data supplied with the polystyrene which also included wavelengths for the principal features (Beckman Instruments, Inc., Irvine, CA). Four weak and a single strong absorption feature labeled 11, 12, 13, 13′, and 13″ are visible on the reference spectrum and have wavelengths listed in Table 3. The Image Reduction and Analysis Facility (IRAF)[1] was used to fit the absorption wavelengths in pixel coordinates and to interpolate the original flux samples onto a linear wavelength grid of 0.109-μm spacing. This procedure was applied to all spectra discussed subsequently. Excerpted values of the wavelength calibration are listed in Table 2 where 45 pixels are seen to be in the useful range of atmospheric transmisison. Calculated pixel wavelengths based on values of $dn/d\lambda$ for NaCl and the spectrometer design are published elsewhere (LeVan and Sloan 1987). The calculated wavelengths are in good relative agreement with the polystyrene calibration discussed here.

The spectral resolution illustrated by the polystyrene spectra is for a relatively large slit width (3″ at the present

[1]IRAF is distributed by National Optical Astronomy Observatories, which is operated by the Association of Universities for Research in Astronomy, Inc., under contract to the National Science Foundation.

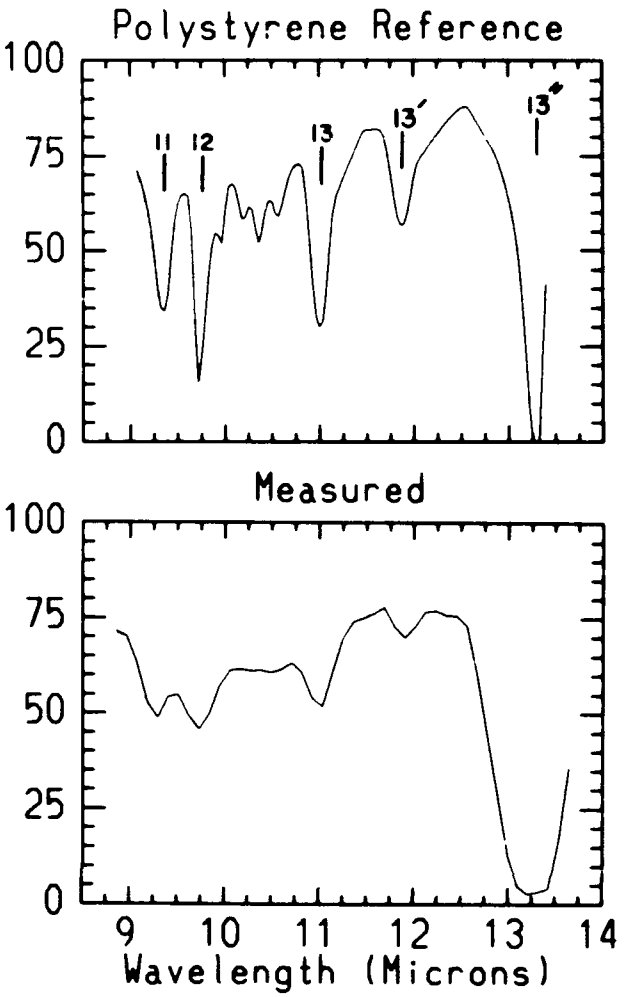

FIG. 3–Spectra of polystyrene calibration film resulting from an exposure of Mars as a background source. Instrumental response and atmospheric transmission variations with wavelength are eliminated in the ratio of spectra with and without polystyrene in the telescope beam (bottom panel). The reference spectrum (top panel) is synthesized from data supplied by the manufacturer of the polystyrene sample. Absorption feature identifications correspond to those of Table 3. The spectral resolution is not optimal since the background source (Mars) was imaged onto a 3″-wide slit and a slit width as small as 1″ may be used under the appropriate conditions of atmospheric seeing. The spectral flux values have been interpolated onto a linear wavelength grid using the IRAF Onedspec package.

TABLE 3

Polystyrene Absorption Wavelengths

Reference	λ(μm)
11	9.35
12	9.73
13	11.03
13′	11.91
13″	13.28

telescope plate scale) installed prior to cryogenically cooling the spectrometer. However, slit widths as small as 1″ may be used under good seeing conditions. Since the spectral resolution using the 3″ slit is an approximate factor of 3 worse than the design goal, one may expect higher resolutions for smaller slit widths.

It is also of interest to note that the polystyrene spectra obtained in June 1988 using Mars as a background source are spatially extended over approximately 10″, simulating a spectrally structured extended source. These spectra exhibit a shift to shorter wavelengths to the north and indicate a rotational misalignment between the slit edges and spectrometer axes as defined by the prism orientation. This misalignment poses no difficulty for point sources and may be easily corrected in extended source observations by using the flux-conserving rotational operations in the IRAF.

3.6 *Flux Calibration*

Observations of bright, variable infrared stars were made at various positions along the spectrometer slit. The relative signals for spectral pixels at a fixed slit position result in correction coefficients for atmospheric and instrumental transmission variations with wavelength, for the "mean" detector responsivity variation with wavelength, and for pixel-to-pixel variations in responsivity. The stellar flux-based calibration is obtained with longer integrations on nonvariable standard stars (e.g., α Bootis, α Tauri, and β Geminorum) at a single position in the slit that overlaps any of the aforementioned positions. Sky-emission measurements were taken at zenith and at larger zenith angles with the telescope chopper off in order to flat field pixels parallel to the slit length. The sky signals are composed of a constant offset term (the telescope background and electronics offsets) and a term proportional to air mass. The difference of the signals at the two air masses is thus proportional to detector responsivity. Relative responses result for monochromatic pixels parallel to the long slit edge. The relative responses of all pixels in the array were set by combining the spectral and spatial calibrations. In practice, the responsivity variation for pixels in the present array is very low (less than 5% rms) which is due in part to the low overall array responsivity (see Table 1).

4. Data Reduction

4.1 *Output Frame Coaddition*

Data frames transferred from the coaddition electronics have been coadded electronically over a 2-sec interval (corresponding to 5 or 7 secondary mirror chop cycles). We define an exposure as 80 such frames, in groups of 20 corresponding to a fixed telescope nod position. Exposures are processed by pair-wise differencing of frames corresponding to the positive and the negative nod positions. The running sum of pair-wise-differenced frames has the residual due to the sky and telescope backgrounds removed (as opposed to the case of coadding the frames in the sequence they were collected). Spikes are eliminated during the coadding, and the number of acceptable values for each pixel is used in the calculation of the average. The sum of the squares of pixel signals is used for the calculation of the standard deviation of the mean. The standard deviations of the mean are the formal uncertainties for subsequent analysis.

4.2 *Atmospheric Correction Coefficients*

An average spectral correction for mean atmospheric and instrumental spectral variations was applied to all pixels in columns perpendicular to the slit long axis. Next, these pixels were multiplied by their unique flat-field coefficients that account for differences from the average spectral correction. Finally, columns of spectral pixels were multiplied by their inverse relative responses as determined by the sky emission flats.

4.3 *Rotational Misalignment Correction*

A 1° misalignment of the prism axes relative to the mosaic array edges results in systematic changes in the slopes of spectral rows of pixels about the peak spectral row. The effects of the rotational misalignment are also evident by shifts of peak spatial emission with wavelength in the amount of 0.012 spatial pixel per spectral pixel. We correct for the misalignment by removing the slope residuals using a model that assumed a Gaussian form for the point-spread function. The functional form for the Gaussian exponent in our model included the usual spatial dependence along with a coupling term between the spatial and spectral axes. The coupling term was determined in a least-squares fashion as the value given above. The Gaussian fit removed both the slope bifurcation and the shift of spatial peak with wavelength.

5. Observational Results

5.1 *Observed Stars*

For the purposes of the present paper we limit our discussion to a set of three stars taken from the larger observing list of LeVan and Sloan (1989). The three stars are representative of three distinct classes: oxygen-rich stars with strong silicate emission (IRC + 10420), carbon stars with silicon carbide emission (V Cygni), and late-type stars having presumed photospheric radiation for which a blackbody spectral distribution is adopted (Arcturus). These three stars were observed on 1988 June 4 UT with at least four exposures (as defined in Section 4.1) each. The absolute flux levels of the spectra were set using the 11-μm flux shown in Figure 4 for Arcturus. The uncertainty in the absolute levels given by repeated exposures is estimated at 25%. We plot the sum of spectra over the spatial point-spread function in Figure 4. Spectra have been regridded on a linear wavelength scale using IRAF, as described in Section 3.5.

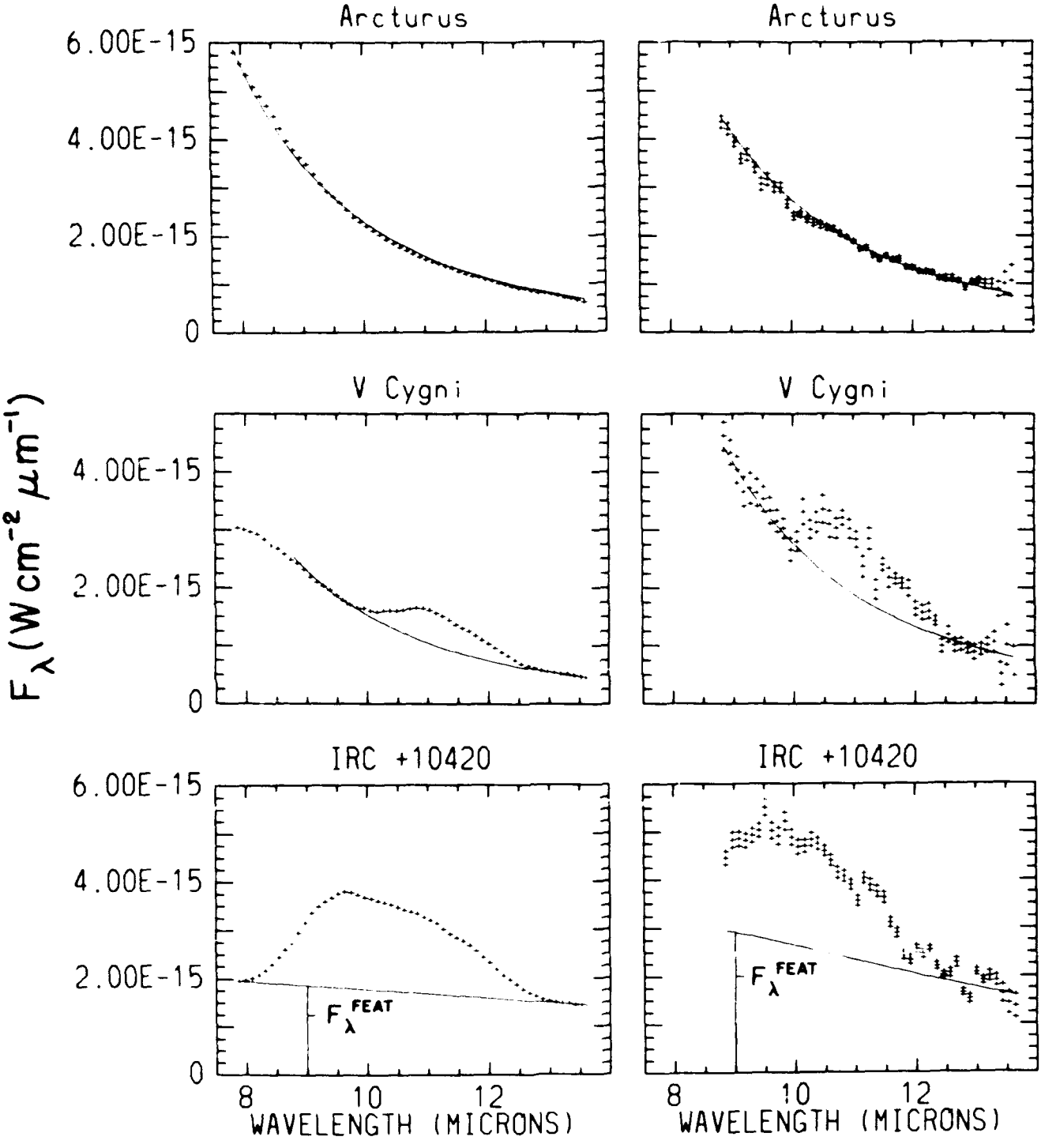

FIG. 4.—Spectra for the three classes of infrared stars observed. Shown are spectra obtained by IRAS (left) and included in the Atlas of IRAS Low Resolution Spectra (Olnon and Raimond 1986) and those obtained with the mosaic array spectrometer (right). The array spectra result from a single mosaic array exposure of two-minutes duration. Peak and subsidiary spectra have been summed over the spatial point-spread function. Blackbody fits to the continua are shown, in the case of Arcturus to aid in evaluating the accuracy of the correction for atmospheric absorption and in the two remaining stars for the comparison of emission feature equivalent widths measured by the two instruments. The blackbody fit for IRC +10420 is based on the ratio of LRS feature and continuum fluxes at the short-wavelength cut-on of the spectrometer, as indicated graphically. Our spectral fluxes have been interpolated onto a linear wavelength grid using the IRAF Onedspec package.

5.2 *Spectra: Comparison with IRAS Low-Resolution Spectra*

In order to evaluate the effectiveness of our data-acquisition and reduction techniques, we compare our spectra with those obtained with the IRAS Low-Resolution Spec-

trometer (LRS) and contained in the Atlas of IRAS Low-Resolution Spectra (Olnon and Raymond 1986, LRS Atlas hereafter). The LRS Atlas includes entries for all three of the stars considered here. First, we note the agreement for the two instruments in the blackbody fit to the continuum of Arcturus. In the cases for the emission feature stars, blackbody fits to the continuum are made for the purpose of comparing the LRS and array spectrometer spectra and are not to be taken as representative of temperatures of either dust grains or the underlying star. Based on the LRS spectrum of the silicate emission star IRC +10420, we see that the continuum blueward of the silicate feature is not sampled by our spectrometer. This is because the wavelength coverage of our instrument is shifted longward to a 9-μm cut-on wavelength as a result of translational misalignment of the optics assembly relative to the mosaic array. At the scale of about 0.1 μm in wavelength per pixel, the observed 1 μm wavelength shift corresponds to about 0.7 mm of translation. For silicate feature spectra observed with the array spectrometer, the blackbody fits to the continua must be chosen such that the short wavelength ratio of feature and continuum levels is equal to that of the LRS spectra at 9 μm. In order to facilitate this procedure we list in Table 4 wavelengths corresponding to a geometric progression of ratios of silicate feature to continuum fluxes obtained from the blackbody fits to the LRS spectra of IRC +10420 and μ Cephei. We note that this feature in the former star, with its larger equivalent width, is also more extended to the shorter wavelengths. The results in Table 4 indicate that for IRC +10420 the silicate feature strength relative to the continuum at 9 μm is approximately 0.75. This ratio is indicated graphically for IRC +10420 in the bottom panels of Figure 4. The correction to the overall feature flux due to feature emission shortward of 9 μm is less than 10% for IRC +10420 and involves a correspondingly small uncertainty. A larger source of uncertainty in the equivalent-width determination results from the placement of the short-wavelength intercept (e.g., a somewhat underestimated continuum level will significantly overestimate the equivalent width). The uncertainty of the reported value of silicate feature equivalent width which combines both corrections is 10%. For μ Cep the value of the feature to continuum ratio at 9 μm is closer to 0.4. The estimation of silicate feature equivalent width for most other stars involves smaller ratios of 9 μm feature to continuum flux than that for IRC +10420 and smaller uncertainties.

TABLE 4

Wavelengths for Fixed Low Resolution Spectra Feature to Continuum Ratios

Star	Feature Equivalent Width (μm)	λ (μm) λ_{FEAT} / F_{CONT} 5%	10%	20%	40%	80%
IRC +10420	3.2	8.14	8.25	8.39	8.63	9.05
μ Cep	2.0	8.34	8.44	8.66	8.97	9.42

For stars exhibiting SiC feature emission (e.g., V Cyg), the spectral coverage of the array spectrometer embraces the continuum both short and longward of the feature. The shapes of the spectra of V Cyg for the two instruments are in satisfactory agreement. The shift in the absolute flux levels exceeds the level of photometric uncertainty and may be attributed to long-period variability (LeVan and Sloan 1989).

A visual comparison between the LRS and array spectrometer spectra indicates the presence of more small-scale structure in the array spectra. This structure reflects the limitations of our correction for atmospheric attenuation and is best quantified by the deviations between the LRS and array spectrometer spectra of Arcturus. The relative smoothness of the LRS spectra results from the absence of residuals from atmospheric correction and the higher sensitivities possible with a cryogenically cooled telescope operated under the lower background levels outside the Earth's atmosphere (Beichman *et al.* 1985).

The standard deviations of the mean of the array spectrometer spectra are large given the 2-minute integration time and the brightnesses of the program stars. Part of the reason for the low signal-to-noise ratio is traceable to the overall low responsivity of the mosaic array (see Table 1), which accounts for perhaps a factor of 5 of the total factor of 200 degradation of our spectrometer relative to the expected sensitivity. Therefore, additional noise sources in our system must account for the majority of the degradation and these are presently under investigation.

5.3 *Spatial Profiles*

The spectral images obtained for the three stars discussed above are useful in the determination of the point-spread function (PSF) of our spectrometer. The experimentally determined PSF can be compared with that expected from the spectrometer design. The profiles displayed in Figure 5 result from summing normalized, monochromatic profiles extracted from single exposures at ten equally spaced wavelengths between 10 and 11.5 μm. The two outermost points have been averaged further over 5 pixels within 2″ of each point. The three profiles shown appear equivalent within the uncertainties and may be characterized by a Gaussian with a σ value of 0.″8. In comparing with our expected value of σ, we use the brightness distribution for diffraction at a circular aperture displayed graphically in Born and Wolf (1964). We note the very good agreement of a Gaussian fit to the primary maximum of the normalized brightness profile down to 5% of peak level, beyond which the first minimum falls sharply below the Gaussian fit. From the Gaussian fit to the calculated diffraction profile at a wave-

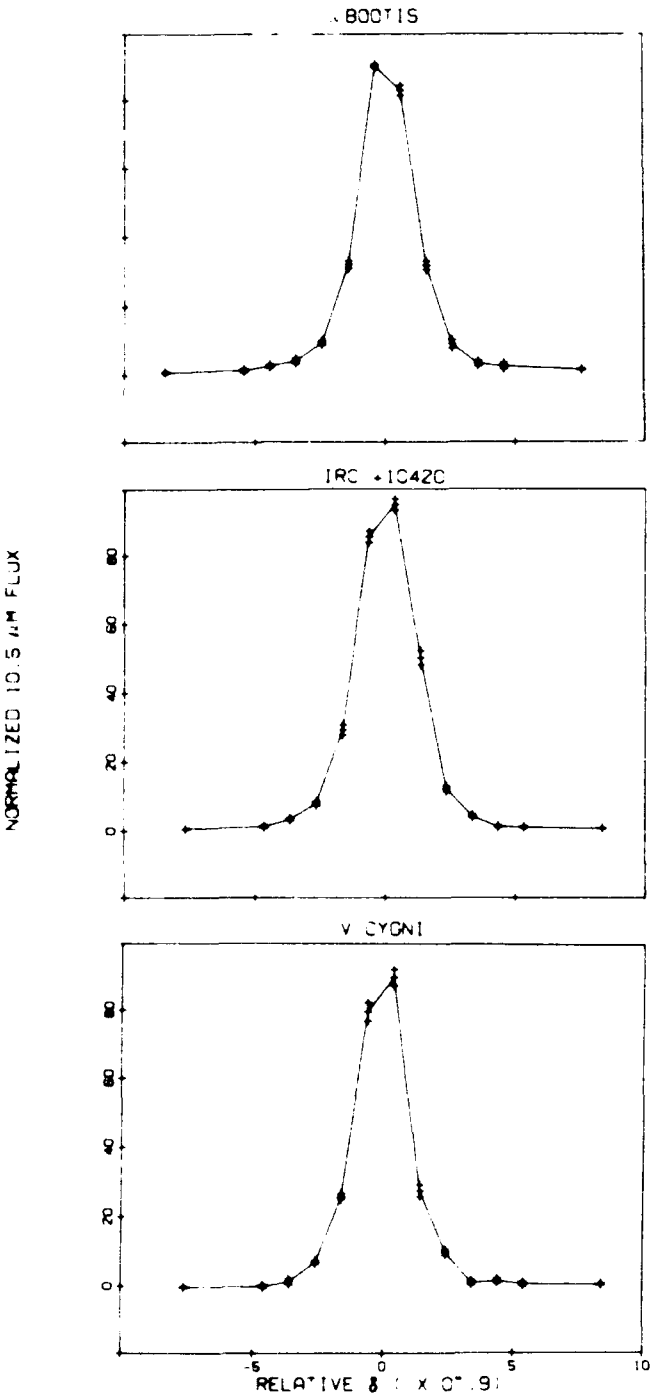

FIG. 5.—Angular profiles obtained at positions along the slit using the same mosaic array exposures as for the spectra shown in Figure 4. These profiles are the sum of ten normalized monochromatic profiles obtained at discrete wavelengths between 10 to 11.5 μm. The two endpoints have been further averaged over 5 pixels within 2" of each endpoint.

length of 11 μm, we find telescope diffraction contributes a Gaussian σ value of 0".39. The spectrometer contribution to the PSF derives from diffraction of the 1-cm-diameter collimated beam at the Lyot stop, and contributes a 33-μm blur (Gaussian σ) on the mosaic array, which corresponds for the array plate scale to 0".38 on the sky. In order to reproduce the observed Gaussian σ value of 0".8, a combination of seeing effects and scattering within the spectrometer in amounts not exceeding 0".4 (Gaussian σ) is required.

6. Conclusions

The evaluation of a slit spectrometer using a mosaic array in the ten-micron region has shown promising results. Spectra were obtained whose qualitative attributes are comparable to those scanned by the IRAS satellite and published in the Atlas of IRAS Low-Resolution Spectra (Olnon and Raimond 1986). The comparison is made for three complementary object classes—oxygen-rich stars with strong silicate feature emission, carbon stars with SiC feature emission, and late-type nonvariable stars with photospheric radiation—and permits the following conclusions: (1) Overall shapes of the IRAS and array spectrometer spectra agree if account is taken of the extension of the silicate feature flux to wavelengths shortward of the 9-μm cut-on wavelength of our instrument. (2) The spectral resolution of our spectrometer matches values expected for the relatively large slit width employed. (3) The width of the spatial point-spread function is close to the design goal but, nevertheless, consistent with either scattering within the spectrometer or a 1" FWHM seeing disk. (4) The noise values of our data points are high even when the relatively low responsivity of the mosaic array is accounted for and are suggestive of non-background-limited performance.

We acknowledge the staff of the Wyoming IR Observatory (WIRO) for providing observational time on the 2.3-m telescope and substantial interface support for the spectrometer described here. WIRO graduate students J. Benson, K. Klett, T. Hayward, and G. Sloan all contributed on various observing runs. Peter Tandy of the Geophysics Laboratory was the electronics engineer responsible for many of the electronics subsystems. Dr. Richard Puetter is gratefully acknowledged for having provided comments leading to the clarification of the original manuscript. This research was supported during its observational phase by the Air Force Office of Scientific Research.

REFERENCES

Arens, J. F., Lamb, G. M., Peck, M. C., Moseley, H., Hoffmann, W. F., Fresch-Fienberg, R., and Fazio, G. G. 1984, *Ap. J.*, **279**, 685
Beichman, C. A., Neugebauer, G., Habing, H. J., Clegg, P. E., and Chester, T. J., eds. 1985, *IRAS Catalogs and Atlases—Explanatory Supplement* (Washington, DC: U.S. Government Printing Office).
Bloemhof, E. E., Townes, C. H., and Vanderwerck, A. H. B. 1984, *Ap. J. Letters*, **276**, L21
Born, M., and Wolf, E. 1964, *Principles of Optics* (New York: MacMillan).
Gehrz, R. D., Hackwell, J. A., and Smith, J. 1976, *Pub. A.S.P.*, **88**, 971
Gezari, D. Y., Folz, W. C., Woods, L. A., and Woolridge, J. B. 1988, *Proc. SPIE*, **973**, 287

LeVan, P. D. 1989, in *Proc. of the Third IR Detector Technology Workshop*, ed. C. R. McCreight (NASA Technical Memo. No. 102209), p. 259
LeVan, P. D., and Sloan, G. 1987, *Proc. SPIE*, **819**, 204
1989, *Pub. A.S.P.*, **101**, 1140
LeVan, P. D., and Tandy, P. C. 1987, *Infrared Astronomy with Arrays*, ed. C. Wynn-Williams and E. E. Becklin (Hilo, HI: University of Hawaii), p. 411 (Paper I)
Olnon, F. M., and Raimond, E. 1986, *Astr. Ap. Suppl.*, **65**, 607 (LRS Atlas)
Tresch-Fienberg, R., Fazio, G. G., Gezari, D. Y., Hoffmann, W. F., Lamb, G. M., Shu, P. K., and McCreight, C. R. 1987, *Ap. J.*, **312**, 542